<Supporting information>

Activating Iodine Redox by Enabling Single-Atom Coordination to Dormant Nitrogen Sites to Realize Durable Zinc–Iodine Batteries

Jisung Lee,[‡a] Wooseok Lee,[‡b] Seungho Back,[‡a] Seung Yeop Yi,[a] Seonggyu Lee,[d, e] Seongseop Kim,[f] Joonhee Moon,[g] Dong-Yeun Koh,[a] Kyeounghak Kim,[c] Seoin Back[b] and Jinwoo Lee*[a]*

[a] Department of Chemical and Biomolecular Engineering, Korea Advanced Institute of Science and Technology (KAIST), Daehak-ro 291, Daejeon 34141, Republic of Korea

[b] Department of Chemical and Biomolecular Engineering, Institute of Emergent Materials, Sogang University, Seoul 04107, Republic of Korea

[c] Department of Chemical Engineering, Hanyang University, 222, Wangsimni-ro, Seongdong-gu, Seoul 04763, Republic of Korea

[d] Department of Chemical Engineering, Kumoh National Institute of Technology (KIT), Gumi 39177, Republic of Korea

[e] Department of Energy Engineering Convergence, Kumoh National Institute of Technology (KIT), Gumi 39177, Republic of Korea

[f] School of Chemical Engineering, Clean Energy Research Center, Jeonbuk National University, Jeonju 54896, Republic of Korea

[g] Division of Materials Analysis, Korea Basic Science Institute (KBSI), Daejeon 34133, Republic of Korea

Email: sback@sogang.ac.kr, jwlee1@kaist.ac.kr

Method

Synthesis of porous N-doped carbon. Porous N-doped carbon (NC) was prepared by direct carbonization of zeolitic imidazole frameworks (ZIF-8) at 1100 ^{o}C. 3.39 g of zinc nitrate hexahydrate was dissolved in 300 ml methanol (solution A). 3.94 g of 2-methylimidazole was dissolved in 300 ml methanol (solution B). After being stirred for one hour until both solutions turned transparent, solution B was swiftly poured into solution A. The resulting mixture was kept stirring for 24 hours at 30 ^{o}C, and then ZIF-8 nanoparticles were collected by centrifugation at 9000 rpm for 10 mins. The collected nanoparticles were washed three times with ethanol and dried overnight at 60 ^{o}C under vacuum condition. The ZIF-8 nanoparticles were subsequently pyrolyzed in a tube furnace under 200 sccm of Ar flow rate at a temperature of 1100 ^{o}C for 2 hours. The resulting products were labeled as NC.

Synthesis of anchored single Ni atom on N-doped carbon (NiNC). The anchored nickel single atom on N-doped carbon (NiNC) was synthesized using a nickel ion adsorption-thermal activation method. First, 100 mg of NC was dispersed in 4 ml methanol under ultrasonication until fully dispersed. Next, a certain amount of nickel nitrate solution (4 mg/ml concentration) was added dropwise into the NC dispersed solution under stirring. After 30 mins ultrasonication and 24 hours stirring, the NC adsorbed with nickel ions was collected by centrifugation at 9000 rpm for 20 mins. The collected products were dried overnight at 60 ^{o}C under vacuum condition, and then thermally activated at 900 ^{o}C for 1 hour to strongly coordinat nickel with N doping sites. The resulting products were denoted as NiNC.

Materials Characterization. The particle morphologies of NiNC and NC before and after iodine loading were observed using a scanning electron microscopy (S-4200 field emission SEM, Hitachi) and a transmission electron microscopy (Tecnai F20 TEM, FEI company). X-ray diffraction (XRD) patterns were obtained using a RIGAKU D/Max-2500 V X-ray diffractometer (Cu Kα radiation, $\lambda = 0.1541$ nm). The N species were investigated by X-ray photoelectron spectroscopy (XPS; Al K-alpha X-ray source, VG Scientific Escalab 250). The nitrogen physisorption was performed at 77 K using a ASAP 2010 (Micromeritics Instrument Co.). High annular dark-field scanning TEM (STEM) and energy dispersive spectroscopy (EDS) were performed for the observation of single Ni atom and further elemental distribution investigation by using a HR-TEM (Titan cubed G2 60-300). The weight of nickel was measured by using a inductively coupled plasma mass spectrometer (7700S ICP-MS, Agilent). X-ray absorption spectroscopy (XAS) analysis was conducted at the XAFS beamline at Pohang Accelerator Laboratory (PAL, Korea). The intermediate species were verified through operando Raman spectroscopy (Ramanforce, Nanophoton) and objective lens Nikon x50 (NA=0.8).

Electrochemical characterization. For electrochemical performance of Zn-I_2 batteries, CR2032-type coin cells were assembled with iodine composites as working electrode, zinc metal foil as counter and reference electrode, and glass fiber as separators. The composites of iodine with AC, NC, and NiNC were prepared by conventional vaporization-condensation method. To fabricate the working electrodes, a slurry was prepared by mixing the iodine composites with each host materials, conductive carbon additive (Super P), and polymeric binder (carboxymethyl cellulose, CMC) in a weight ratio of 8:1:1 using a solvent (DI water).

The prepared slurry was coated on Ti foil, and dried at 60 °C for 6 h. The electrolyte was the 2 M solution of zinc sulfate ($ZnSO_4$). The electrolyte-to-iodine (E/I) ratio is fixed to 50 for all the galvanostatic analysis. The galvanostatic electrochemical test was assessed by WBCS-3000 battery cycler (Wonatech Co., Korea) in the potential range between 0.4 and 1.6 V (vs. Zn/Zn^{2+}) at different current densities from 0.2 A g^{-1} to 6 A g^{-1}. The capacity was calculated based on the iodine weight in the electrode. Cyclic voltammetry (CV) was conducted using VSP potentiostat (Bio-Logic co.) with a scan rate from 0.1 mV s^{-1} to 1 mV s^{-1}.

Computational Details. We performed spin-polarized density functional theory (DFT) calculations using Vienna ab-initio simulation package (VASP) version 5.4.4 with the generalized gradient approximation (GGA)−Perdew-Burke-Ernzerhof (PBE) exchange-correlation functional and projector augmented wave (PAW) pseudopotential. Grimme's D3 correction was applied to include van der Waals interactions. A plane wave cutoff energy of 500 eV was used, and convergence tolerances for energy and force were set to10^{-5} eV and 0.05 eV $Å^{-1}$, respectively. We calculated adsorption energies (E_{ads}) of iodine species on C, NC and NiNC as $E_{ads} = E_{total} - E_{surface} - E_{adsorbate}$, where E_{total}, $E_{surface}$ and $E_{adsorbate}$ are DFT calculated electronic energies of iodine species adsorbed on surface, bare surface and iodine species, respectively. The DFT energy of iodine species was calculated in 15 Å × 15 Å × 15 Å unit cell. More negative values indicate more favorable interactions. The charge density difference ($\Delta\rho$) was calculated as $\Delta\rho = \rho_{total} - \rho_{adsorbate} - \rho_{surface}$, where ρ_{total}, $\rho_{adsorbate}$ and $\rho_{surface}$ represent the charge densities of the total system, the adsorbate and the bare surface, respectively. The isosurface level was set to 0.007 e/$Bohr^3$, where the yellow (cyan) indicates charge accumulation (depletion). The Crystal Orbital Hamilton Population (COHP) analysis was

performed using the LOBSTER package to analyze the binding properties of I_2 molecules, with a focus on the electronic interactions between I atoms. This approach allows the discrimination of bonding and antibonding states based on the density of states, thus enabling the estimation of bonding strength through the integration of COHP up to the Fermi level (ICOHP).

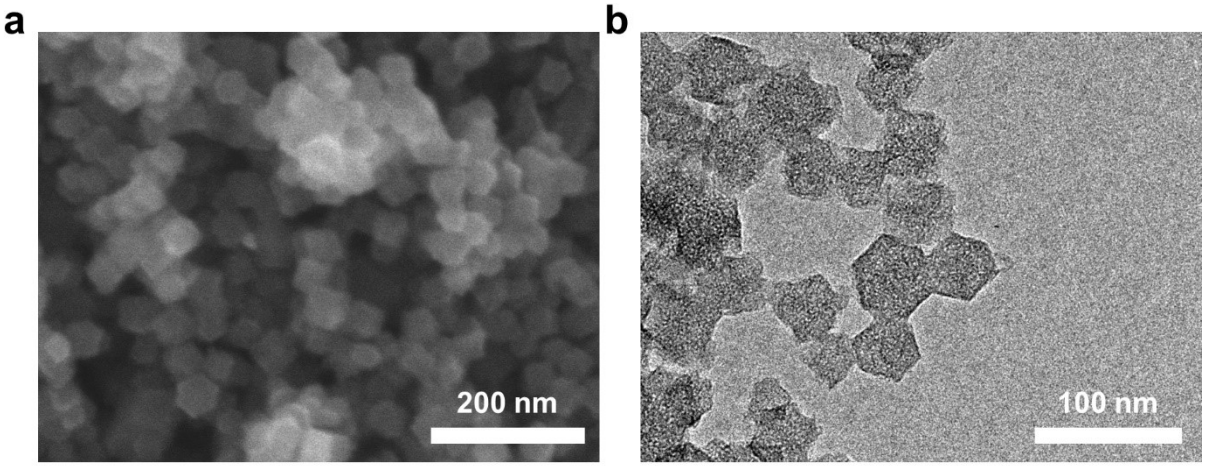

Fig. S1 (a) SEM and (b) TEM micrographs of N-doped carbon (NC) derived from carbonized ZIF-8.

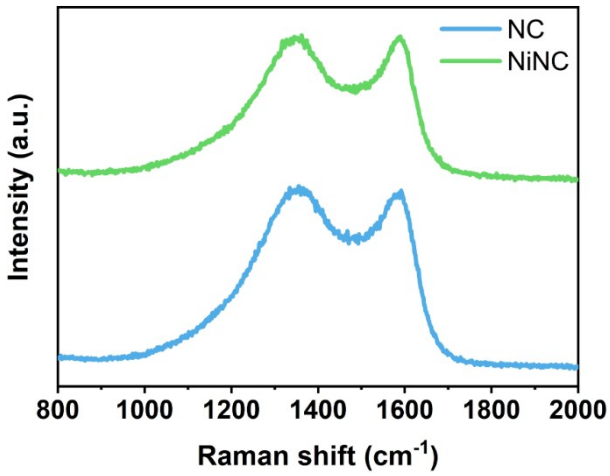

Fig. S2 Raman spectra of NC and NiNC.

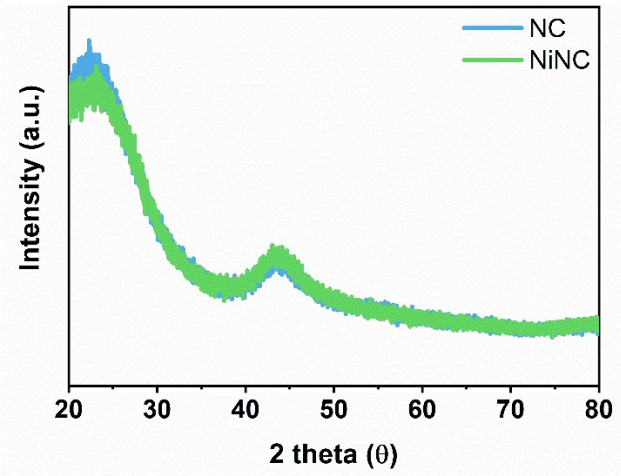

Fig. S3 The powder XRD patterns of NC and NiNC.

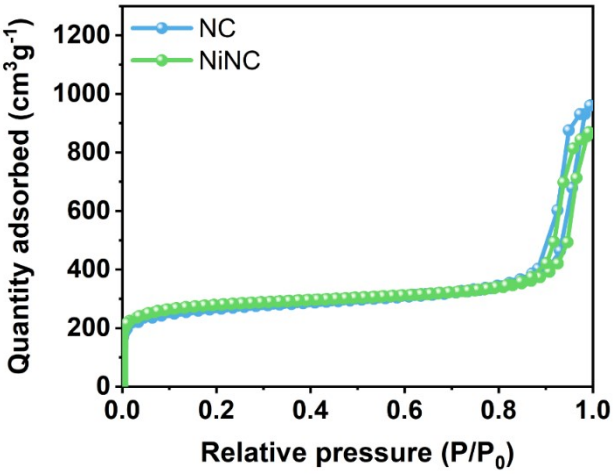

Fig. S4 N_2 physisorption isotherms of NC and NiNC.

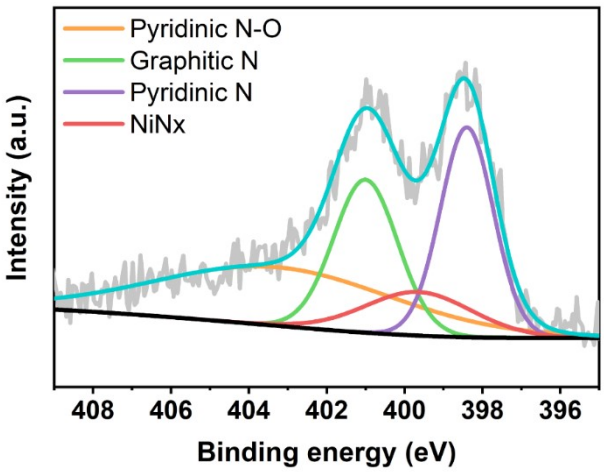

Fig. S5 High-resolution XPS spectra of N 1s for NiNC.

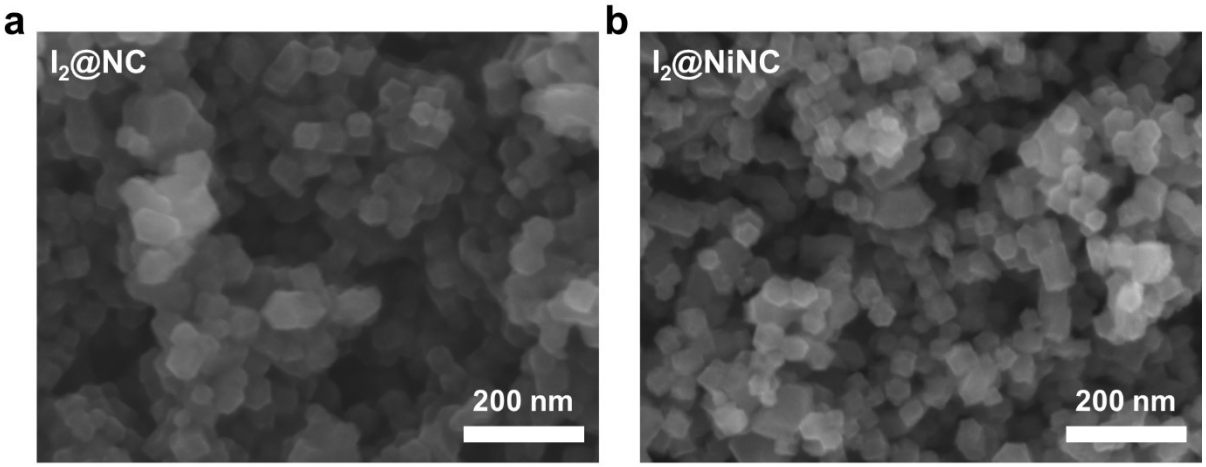

Fig. S6 SEM images of (a) NC and (b) NiNC after iodine loading.

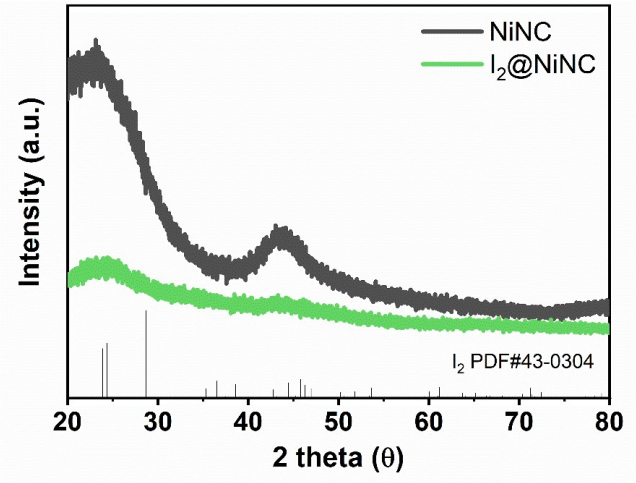

Fig. S7 Powder XRD patterns of NiNC before and after iodine loading.

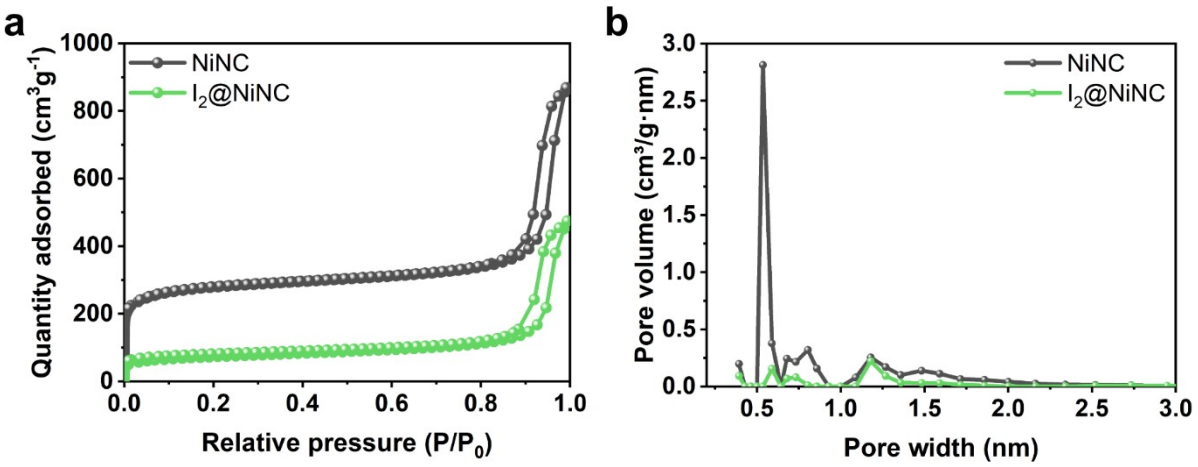

Fig. S8 (a) N_2 physisorption isotherms and (b) pore size distribution curve of NiNC before and after iodine loading.

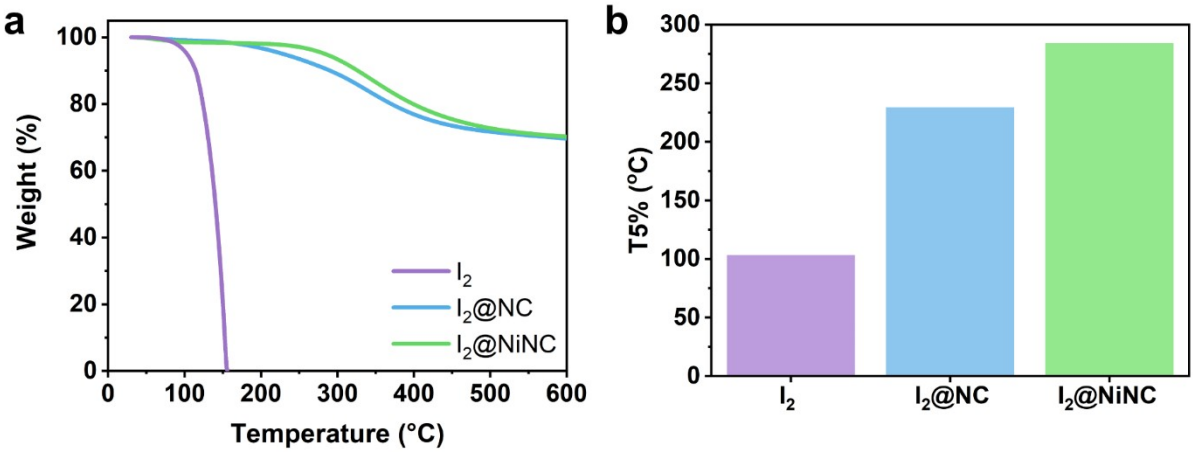

Fig. S9 (a) Thermogravimetric curves and (b) comparison of T5% of I_2, I_2@NC, and I_2@NiNC.

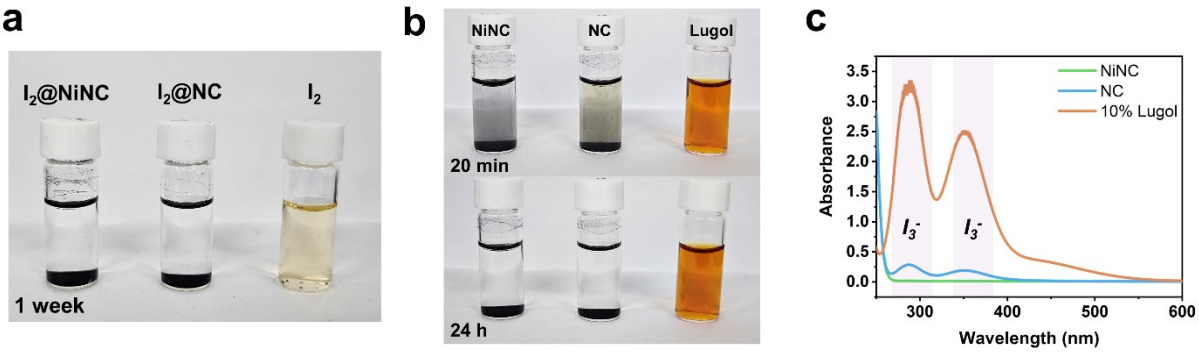

Fig. S10 (a) Digital photos of stability test in 2M $ZnSO_4$ electrolyte (after 1 week). (b) Digital photos for adsorption test of NC and NiNC in Lugol solution after 20 mins (upper) and 24 hours (bottom). (c) The UV-vis spectra of NC and NiNC in Lugol solution after 24 hours.

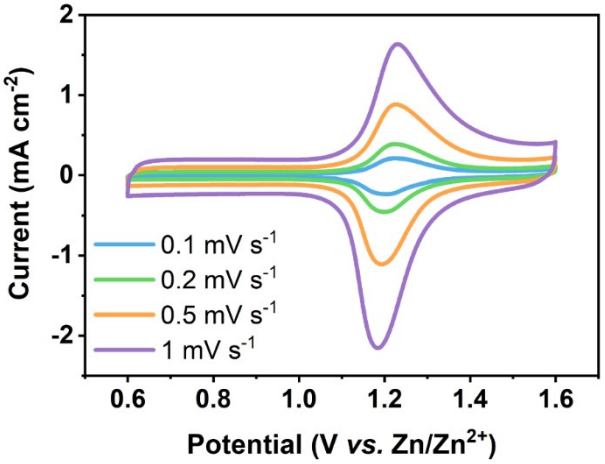

Fig. S11 Cyclic voltammetry curves of I_2@NiNC cathode at various scan rates in range of 0.6 – 1.6 V.

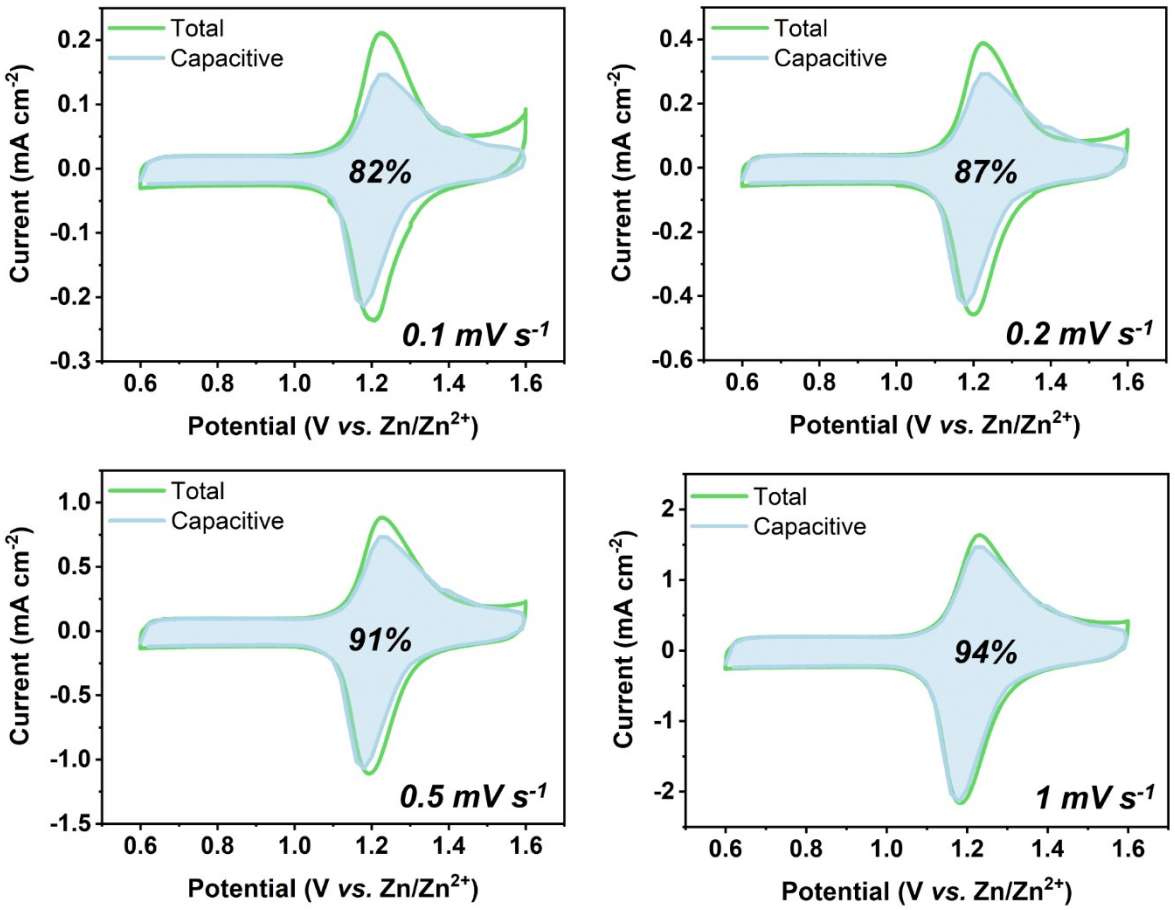

Fig. S12 Surface-induced capacitive reaction contribution of I_2@NiNC at various scan rates of 0.1, 0.2, 0.5, and 1 mV s^{-1}.

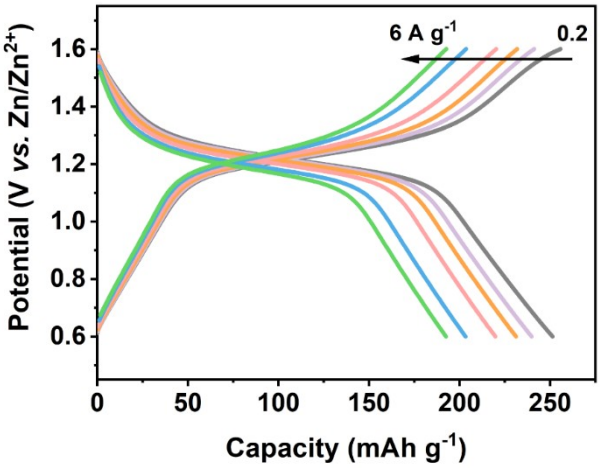

Fig. S13 Galvanostatic charge-discharge curves of I_2@NiNC at various current densities (0.2, 0.5, 1, 2, 4, and 6 A g^{-1}).

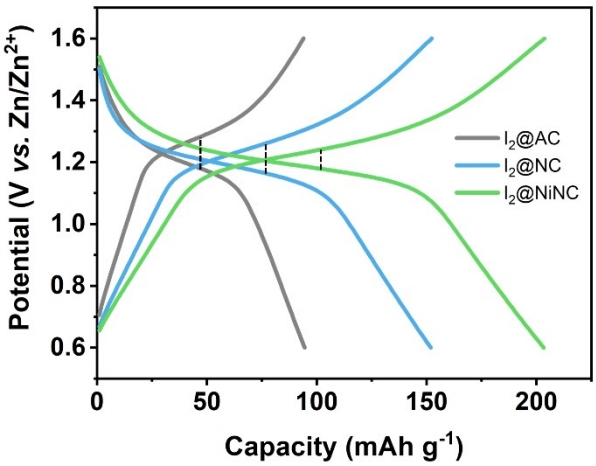

Fig. S14 Galvanostatic charge-discharge curves of I_2@AC, I_2@NC, and I_2@NiNC at a current density of 4 A g^{-1}, showing distinct polarization voltage values at half capacity.

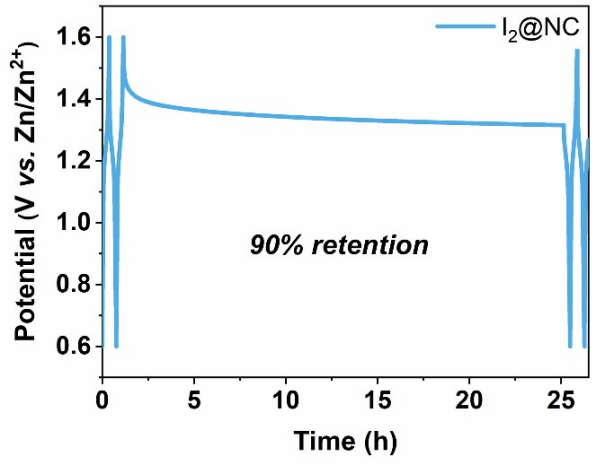

Fig. S15 Self discharge curve of I_2@NC resting for 24 h after being fully charged.

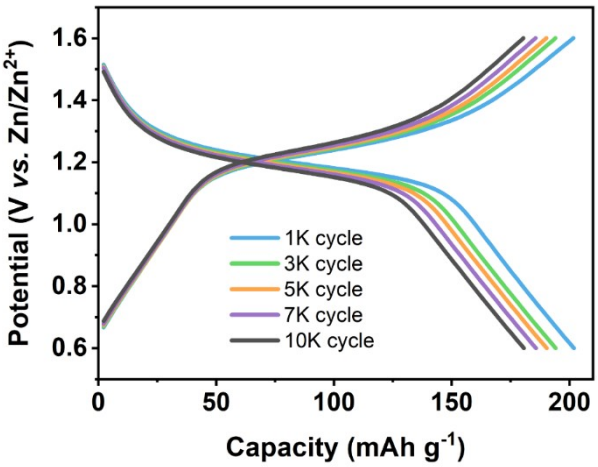

Fig. S16 Galvanostatic charge-discharge curves at a current density of 6 A g^{-1} for various cycles: 1K, 3K, 5K, 7K, and 10K (where 1K = 1000 cycles).

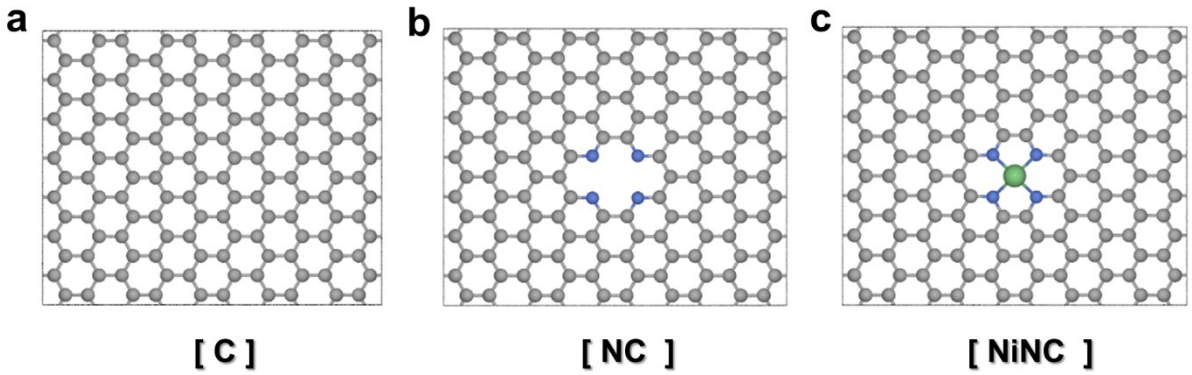

Fig. S17 Top views of the optimized structures of (a) C, (b) NC and (c) NiNC. Color codes: grey (C), blue (N), and green (Ni).

We modelled three structures using (5 × 7) supercell of graphene, referred to as C, NC and NiNC. The C, NC and NiNC correspond to graphene, defective graphene with four pyridinic N atoms and Ni single-atom site with four neighboring N atoms, respectively. 30 Å of a vacuum layer was added in *z*-direction to avoid an artificial interaction between periodic images. The parameters of the supercell are 21.38 Å × 17.27 Å × 30.00 Å. Gamma-centered (1 × 1 × 1) k-point was sampled for all structures.

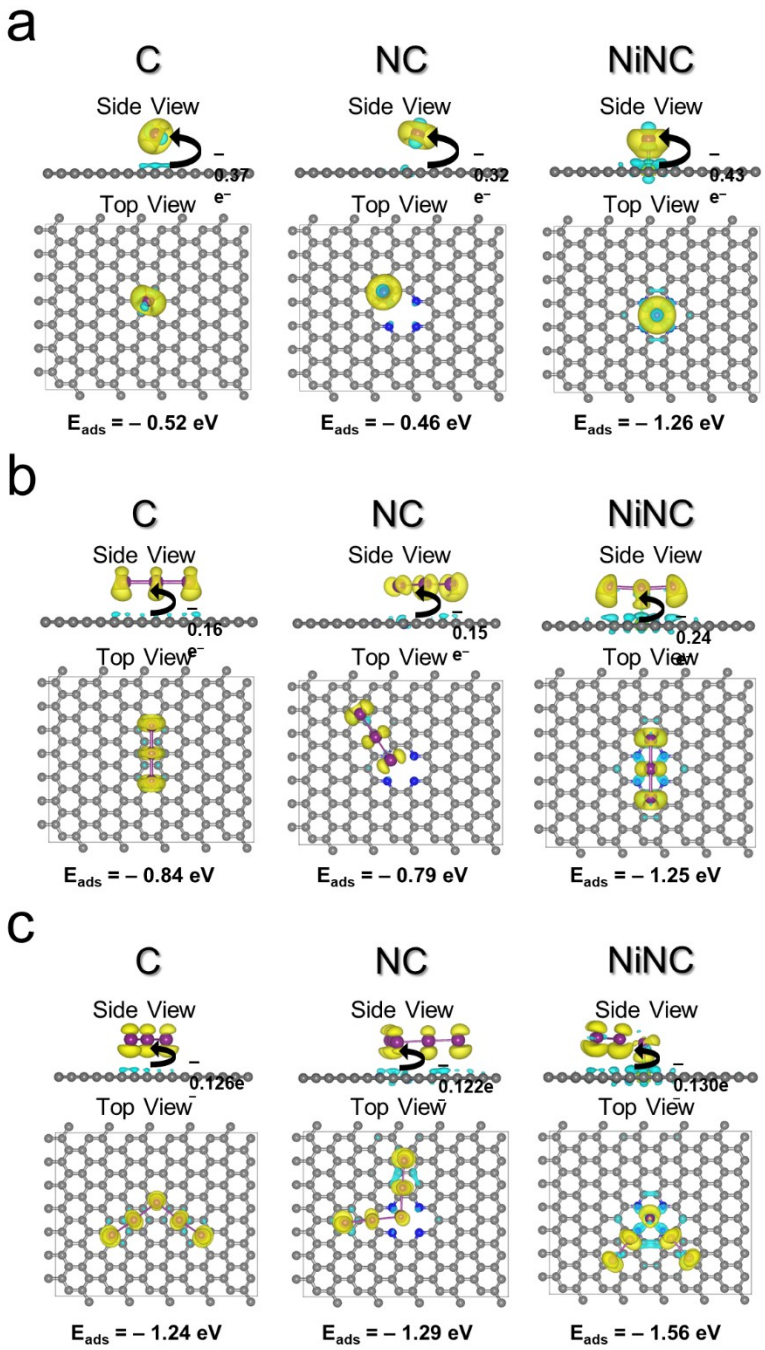

Fig. S18 Charge density difference plot during the adsorption of (a) I^-, (b) I_3^- and (c) I_5^- on C, NC and NiNC. The amounts of electron transfer calculated from the Bader Charge analysis and I–I intermolecular distance are also displayed. Color codes: purple (I), grey (C), blue (N), green (Ni).

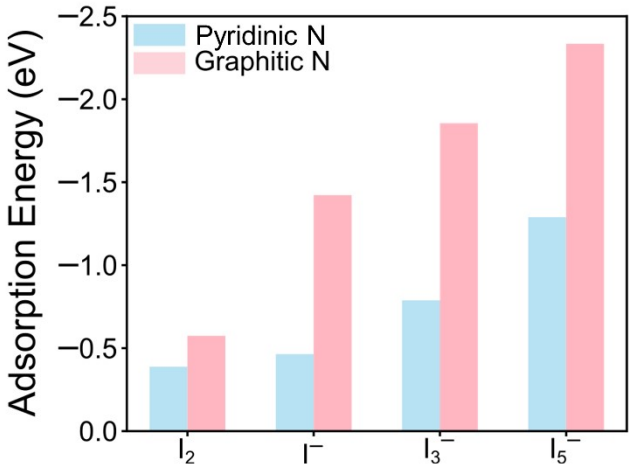

Fig. S19 Adsorption energies of I_2, I^-, I_3^- and I_5^- on pyridinic N (blue) and graphitic N (red).

Table S1. Surface area and micropore volume comparison of NC, NiNC, and I_2@NiNC.

	NC	**NiNC**	**I_2@NiNC**
Surface area (m^2 g^{-1})	855	1047	263
Micropore volume (cm^3 g^{-1})	0.25	0.34	0.05

Table S2. Element contents of NiNC and detailed XPS data for N 1s.

Element contents (at%)				
	C	**N**		**O**
NiNC	91.19	5.53		3.16
	Pyridinic N	**Ni-N_x**	**Graphitic N**	**Pyridinic N-O**
Peak center (eV)	398	399	401	403
% of total N 1s	28.6	12.4	25	34

Table S3. EXAFS results for NiNC catalysts modulating the defect site.

	Path	CN	R(Å)	σ^2(Å^2)	ΔE0 (eV)	R factor (%)
NiNC	Ni-N	4.03	1.87(8)	0.004(8)	9.4(9)	0.45

CN: coordination number; R: interatomic distance; σ^2: Debye-Waller factor that is related to thermal and static disorder in absorber-scatterer distances; ΔE_0: edge-energy shift; R-factor: represents the goodness of the fitting; the amplitude reduction factor S_0^2 was determined to be 0.84 obtained using Ni foil fitting as a reference.

Table S4. Ni elemental quantification of NiNC by ICP-MS (wt.%).

	NiNC
Ni (wt. %)	1.1

Table S5. Comparison of the electrochemical performance between the I_2@NiNC electrode and state-of-the-art carbonaceous host materials reported in literature.

Cathode material	Rate capability	Cyclability	Reference
NiNC/I_2	255 mA h g^{-1}@0.2 A g^{-1} 241 mA h g^{-1}@0.5 A g^{-1} 232 mA h g^{-1}@1 A g^{-1} 221 mA h g^{-1}@2 A g^{-1} 204 mA h g^{-1}@4 A g^{-1} 193 mA h g^{-1}@6 A g^{-1}	207 mA h g^{-1}@1 A g^{-1} after 2000 cycles 181 mA h g^{-1}@4 A g^{-1} after 10000 cycles	This work
Active carbon fiber cloth/I_2 (ACFC)	174 mA h g^{-1}@0.106 A g^{-1} 155 mA h g^{-1}@0.211 A g^{-1} 143 mA h g^{-1}@0.422 A g^{-1} 124 mA h g^{-1}@1.06 A g^{-1}	162 mA h g^{-1}@0.211 A g^{-1} after 300 cycles 131 mA h g^{-1}@0.422 A g^{-1} after 3000 cycles	[1]

N-doped carbon/I_2 (NC)	261.3 mA h g^{-1}@0.211 A g^{-1} 228.5 mA h g^{-1}@0.422 A g^{-1} 200.1 mA h g^{-1}@1.06 A g^{-1} 177.7 mA h g^{-1}@2.11 A g^{-1} 154.6 mA h g^{-1}@4.22 A g^{-1}	133 mA h g^{-1}@2.11 A g^{-1} after 10000 cycles	[2]
Graphitic N-doped carbon/I_2 (G-NC)	250 mA h g^{-1}@0.2 A g^{-1} 224 mA h g^{-1}@0.4 A g^{-1} 208 mA h g^{-1}@1 A g^{-1} 185 mA h g^{-1}@2 A g^{-1} 175 mA h g^{-1}@4 A g^{-1}	205 mA h g^{-1}@0.4 A g^{-1} after 6000 cycles 142 mA h g^{-1}@1 A g^{-1} after 10000 cycles	[3]
Mesoporous carbon/I_2 (MPC)	116 mA h g^{-1}@0.2 A g^{-1} 109 mA h g^{-1}@0.5 A g^{-1} 105 mA h g^{-1}@1 A g^{-1} 98 mA h g^{-1}@3 A g^{-1} 90 mA h g^{-1}@5 A g^{-1}	99 mA h g^{-1}@0.5 A g^{-1} after 1000 cycles 57 mA h g^{-1}@10 A g^{-1} after 39000 cycles	[4]

Fe-N-C porous carbon/I_2 (FeNPC)	220 mA h g^{-1}@0.211 A g^{-1} 158 mA h g^{-1}@4.22 A g^{-1}	180 mA h g^{-1}@1.06 A g^{-1} after 5000 cycles 168 mA h g^{-1}@2.11 A g^{-1} after 10000 cycles	[5]
Defect rich carbon/I_2 (DC)	278.4 mA h g^{-1}@0.5 A g^{-1} 263.2 mA h g^{-1}@1 A g^{-1} 238.1 mA h g^{-1}@2 A g^{-1} 194.6 mA h g^{-1}@4 A g^{-1} 164.1 mA h g^{-1}@6 A g^{-1} 144.4 mA h g^{-1}@8 A g^{-1} 131.9 mA h g^{-1}@10 A g^{-1}	261.4 mA h g^{-1}@1 A g^{-1} after 3500 cycles	[6]
MOF-5 derived carbon/I_2 (M5C)	120 mA h g^{-1}@1 A g^{-1} 107 mA h g^{-1}@2 A g^{-1} 94 mA h g^{-1}@3 A g^{-1} 82 mA h g^{-1}@4 A g^{-1} 74 mA h g^{-1}@5 A g^{-1}	137 mA h g^{-1}@0.1 A g^{-1} after 300 cycles 112 mA h g^{-1}@1 A g^{-1} after 2000 cycles	[7]

Supplementary References

1. H. Pan, B. Li, D. Mei, Z. Nie, Y. Shao, G. Li, X. S. Li, K. S. Han, K. T. Mueller and V. Sprenkle, *ACS Energy Lett.*, 2017, **2**, 2674-2680.
2. D. Yu, A. Kumar, T. A. Nguyen, M. T. Nazir and G. Yasin, *ACS Sustain. Chem. Eng*., 2020, **8**, 13769-13776.
3. T. Liu, H. Wang, C. Lei, Y. Mao, H. Wang, X. He and X. Liang, *Energy Stor. Mater*., 2022, **53**, 544-551.
4. Q. Guo, H. Wang, X. Sun, Y. n. Yang, N. Chen and L. Qu, *ACS Mater. Lett*., 2022, **4**, 1872-1881
5. M. Liu, Q. Chen, X. Cao, D. Tan, J. Ma and J. Zhang, *J. Am. Chem. Soc*., 2022, **144**, 21683-21691.
6. S. Niu, B. Zhao and D. Liu, *ACS Appl. Mater. Interfaces*, 2023, **15**, 25558-25566.
7. Y. Hou, F. Kong, Z. Wang, M. Ren, C. Qiao, W. Liu, J. Yao, C. Zhang and H. Zhao, *J. Colloid Interface Sci*., 2023, **629**, 279-287.